Synthesis of nanosized MFI zeolites using Cu-containing complexes

Peng Peng, Simona Moldovan, Aurélie Vicente, Valérie Ruaux, Maxime Debost, Han Hu, Hristiyan Aleksandrov, Georgi Vayssilov, Zi-Feng Yan, Svetlana Mintova

Synthesis of nanosized MFI zeolites using Cu-containing complexes

Peng Peng [a,b], *Simona Moldovan* [c], *Aurélie Vicente* [b], *Valérie Ruaux* [b], *Maxime Debost* [b], *Han Hu* [a], *Hristiyan A. Aleksandrov* [d], *Georgi N. Vayssilov*[d], *Zi-Feng Yan* [*a], *and Svetlana Mintova* [*a,b]

[a] State Key Laboratory of Heavy Oil Processing, China University of Petroleum, Qingdao 266580, China.
[b] Laboratoire Catalyse et Spectrochimie (LCS), Normandie Univ, ENSICAEN, UNICAEN, CNRS, 14000 Caen, France.
[c] Groupe de Physique des Matériaux, CNRS, Université Normandie & INSA Rouen, 76801 St Etienne du Rouvray, France.
[d] Faculty of Chemistry and Pharmacy, University of Sofia, 1126 Sofia, Bulgaria.

*Corresponding authors: E-mail address: zfyancat@upc.edu.cn and svetlana.mintova@ensicaen.fr

Abstract

Nanosized MFI type zeolites were synthesized in the presence of Cu-containing complexes. The use of ethylene diamine tetraacetic acid (EDTA) as a ligand promoted the solubility and guaranteed the exclusive configuration of the copper-bearing chelate in the precursor solutions. The EDTA-assisted MFI zeolite nanocrystals (Cu-MFI-EDTA) was found to contain low amount of silanols due to formation of flexible Si-O-Cu bonds. On the contrary, when ammonia (NH_3) was used as a ligand, the copper species in the sample (Cu-MFI-NH_3) only present in the form of extra framework $[Cu^{\delta+}\cdots O^{\delta-}\cdots Cu^{\delta+}]_n$ clusters. The introduction of transition metals assisted by ligands permitted the preparation of nanocrystals with variable amount of silanols and modified water affinity.

Keywords: Nanosized zeolite; Silanols; Copper complexes; Ethylene diamine tetraacetic acid

1. Introduction

Zeolite is crystalline microporous material consisting of 3D-connected tetrahedrally coordinated (T) atoms (T = Si, Al, P, *etc*.).[1] Thanks to the tunable chemical composition, high thermal stability and surface acidity, zeolite is becoming a "game-changer" in the field of renewable energy and environmental improvement.[2] In addition, via decreasing the size of the crystals from micron- to nano-scale, the external surface area and diffusion are consistently increased.[3–5] However, accompanied with the benign properties brought from nanosized zeolites, the amount of silanols inside and/or outside the zeolite crystals is also inevitably increased.[6–8] Such silanols sites are originated from the missing framework atoms in the zeolite structure formed either during the synthesis or post-synthesis treatments.[9] The silanol groups prefer to interact with water molecules to form "small H_2O clusters"[10], lowering the hydrothermal stability of zeolites under harsh conditions.[11] From this point, healing silanols is of interest to both improve zeolite stability and decrease the water affinity.

Introducing transition metals into the framework of nanosized zeolite during synthesis is a newly-developed environmentally-friendly approach to cope with the above-mentioned problems.[12] On one hand, the silanols in zeolites were reported to be efficiently healed after adding transition metal species.[13–15] On the other hand, when transition metals are inserted in the zeolite framework, they are less likely to be sintered.[16]

Although metal incorporation has received more and more attentions, the used transition metal precursors were still restricted to the oxoacid anions. The synthesis of (alumino)silicate zeolite is usually carried out under alkali conditions. The oxoacid anions can maintain high solubility under alkali synthesis conditions for zeolites and are not prone to precipitate. However, Cu usually exists in the form of hydrated cupric cations in aqueous solutions. In such case, the cations easily precipitate with hydroxide anions **(Fig. S1(A) in Supporting Information (SI))**. For this reason, effectively incorporating Cu species, which has shown advantages in the field of catalysis such as selective oxidation of methane into methanol [17], selective catalytic reduction (SCR) of NO_x emission [18], *etc*., is an interesting and is still a challenging task.[19]

Herein, a one-pot synthetic strategy for nanosized MFI zeolites via Cu-containing complexes is reported.

2. Experimental Section

2.1 Chemicals

Tetrapropyl ammonium hydroxide (TPAOH, 1.0 mol/L aqueous solution) and copper sulfate pentahydrate ($CuSO_4 \cdot 5H_2O$, >99 wt%) were purchased from Alfa Aesar Co. Ltd. Tetraethyl orthosilicate (TEOS, 98 wt%), and ethylene diamine tetra acetic acid disodium salt (EDTA, >98 wt%) were purchased from Sigma-Aldrich Co. Ltd. All the reagents were used without further purification.

2.2 Synthesis

2.2.1 Synthesis of copper-containing MFI nanosized zeolite with EDTA ligand (sample Cu-MFI-EDTA)

Specifically, 9.8 g TPAOH, 0.055 g $CuSO_4 \cdot 5H_2O$, and 0.165 g EDTA were mixed and stirred for 2.5 hours. Afterwards, 5 g TEOS and 0.857 g double distillated water were added sequentially. The precursor mixture was stirred at room temperature for 3 hours and then placed on a shaker (250 rpm) for 16 hours to form a cerulean transparent suspension **(Fig. S1(B) in Supporting Information).** Then the precursor mixture was heated in an oven at 90 ^{o}C for 160 hours. In order to easily monitor the hydrothermal crystallization process, the above precursor mixture was sealed in a polypropylene (PP) bottle. Then the product was centrifuged, washed, dried. Finally, the as-synthesized sample was calcinated at 550 ^{o}C for 6 hours. The SEM images and related histograms of Cu-MFI-EDTA are shown in **Fig. S2(A)**. The results unambiguously confirm that the Cu-MFI-EDTA sample contains nanosized crystals with a mean particle diameter of 90.1 nm.

2.2.2 Synthesis of copper-containing MFI nanosized zeolite with ammonia ligand (sample Cu-MFI-NH_3)

In a typical synthesis process: 9.8 g TPAOH, 0.055 g $CuSO_4 \cdot 5H_2O$, 2.556 g NH_4OH mixed and stirred for 2.5 hours. Afterwards, 5 g TEOS was added drop by drop and then 0.857 g double-distillated water was added at once. The resulted precursor mixture was stirred at room temperature for 3 hours and then placed on a shaker (250 rpm) for

16 hours to form a violet transparent suspension **(Fig. S1(C) in Supporting Information).** The precursor mixture was then heated in an oven at 90 ^{o}C for 48 hours. In order to avoid the possible volatilization of ammonia at 90 ^{o}C and the consequent impact on the crystallization process, the above mixture was sealed in a stainless-steel autoclave with a Teflon-lined container. The product was purified and dried and calcinated at 550 ^{o}C for 6 hours. The SEM images and related histograms of Cu-MFI-NH_3 are shown in **Fig. S2(B)**. The results unambiguously confirm that the Cu-MFI-NH_3 sample contains nanosized crystals with a mean particle diameter of 135.2 nm.

2.2.3 Synthesis of pure siliceous nanosized silicalite-1 (reference sample Si-MFI)

The reference Si-MFI nanosized zeolite was prepared using the same precursor suspension as the one used for synthesizing nanosized Cu-MFI-EDTA and Cu-MFI-NH_3 zeolites, without introducing $CuSO_4 \cdot 5H_2O$, EDTA or NH_4OH. In a typical synthesis process: 5 g TEOS was added drop by drop into 9.8 g TPAOH. Then 0.857 g double-distillated water was added at once. The precursor mixture was subjected to stirring at room temperature for 3 hours and then placed on a shaker for 16 hours. The colorless transparent precursor mixture was heated in an oven at 90 ^{o}C for 26 hours. In order to easily monitoring the hydrothermal crystallization process, the above mixture was sealed in a PP bottle. After crystallization, the product was purified, dried and calcined using the same procedure described above. The SEM images and related histograms of Si-MFI are presented in **Fig. S2(C)**. The results unambiguously

confirmed that the Si-MFI sample contains nanosized crystals with a mean particle diameter of 83.5 nm.

2.3 Characterizations

The thermogravimetry analysis (TG) were conducted by a SETARAM SETSYS-B microbalance with sensitivity of 0.1 μg. All the samples were calcinated before conducting water adsorption tests to make sure that all the organics have been removed. The conditions for water adsorption were referred and modified from an ASTM standard (ASTM D5758-01 2015). Specifically, the finely grinded samples were firstly placed into an oven at 105 ^{o}C for 16 hours for removing pre-adsorbed water and other impurities. Afterwards, they were transferred into a desiccator maintained at 58 % relative humidity via saturated sodium bromide aqueous solution and stored at 25 ^{o}C for 72 hours.

The silanol group vibration modes of zeolite were characterized using a Nicolet Magna 550-FTIR spectrometer with 2 cm^{-1} optical resolution equipped with an *in-situ* cell. The self-supported zeolite wafers were evacuated (1.33×10^{-4} Pa) and pretreated at 450 ^{o}C for 4 hours prior the measurements, and then the spectra were collected in the region of 4000-3000 cm^{-1}.

^{29}Si magic angle spinning nuclear magnetic resonance (^{29}Si MAS NMR) and {^{1}H}-^{29}Si cross-polarized magic angle spinning nuclear magnetic resonance ({^{1}H}-^{29}Si CP MAS NMR) were conducted on a Brucker Avance III-HD 500 (11.7 T) spectrometer using a zirconia rotor with a diameter of 4 mm. The spinning frequency of the rotor was fixed

to 12 kHz. For ^{29}Si MAS NMR, the spectrometer was operated at 99.3 MHz, and a single pulse excitation (30^{o} flip angle) was used with a recycle delay of 30 seconds. While for {^{1}H}-^{29}Si CP MAS NMR, a contact time of 5 mi and a recycle delay of 2 seconds were used. Tetramethylsilane (TMS) was used as a reference for measuring ^{29}Si chemical shifts.

Powder X-ray diffraction (XRD) patterns were recorded by a PANalytical X'Pert PRO MPD diffractometer equipped with Cu Kα radiation (45 kV, 40 mA, λ = 0.1541 nm) in the 2theta range of 3-80^{o}. The unit cell parameters of the samples were calculated from their XRD patterns using JANA2006 software where Le Bail profile refinement, and pseudo-Voigt function were selected.

Raman spectra were collected on a Jobin Yvon Labram 300 confocal Raman spectrometer coupled with a microscope (objective: 50×) and a CCD detector. A 532 nm wavelength laser was used, and the spectra were accumulated 3 times for 60 seconds each.

The structural vibration modes of zeolite framework were collected using a Nicolet Magna 550-FTIR spectrometer with 2 cm^{-1} optical resolution. Before testing, all samples were mixed with potassium bromide and then pressed into self-supported wafers.

UV-Vis spectra were recorded using a Varian Cary 4000 UV-Vis-NIR spectrometer in the range from 800 to 200 nm. Prior to the tests, the sample powders were placed into a

cell equipped with a quartz window; magnesium hydroxide was used as a reference sample.

Scanning transmission electron microscopy (STEM) and Energy Dispersive Spectroscopy (EDS) were performed using a double corrected JEOL ARM200 CFEG TEM operated at 80 kV (to avoid the specimen damage by electron beam irradiation) equipped with a 100 mm^2 Centurio detector for the X-rays. For the imaging, the High Angular Annular Dark Field (HAADF) detector was employed in order to accede the *Z* chemical contrast in the imaging mode. A probe current of 0.1 nm was employed to acquire images of 1024 × 1024 px at a speed of 12 µs/px. 256 × 256 px EDS chemical maps were continuously acquired with an exposure of 0.02 ms/px and a cross-correlation algorithm was applied to correct for the spatial drift every 30 seconds. The nitrogen monoxide (NO) adsorption on the zeolite samples was followed using a Nicolet Magna 550-FTIR spectrometer with 2 cm^{-1} optical resolution with an *in situ* cell. Prior the measurements, the self-supported zeolite wafers were evacuated (1.33×10^{-4} Pa) and pretreated at 450 ^{o}C for 4 hours. Then the spectra were collected at room temperature (RT) under delivering different NO concentrations (3.0, 5.9, 8.9, 11.8, 14.7, and 17.6×10^{-3} mmol/g).

2.4 Density functional theory (DFT) calculations

Periodic DFT calculations were performed using the Perdew-Burke-Ernzerhof (PBE) [20], exchange-correlation functional as the dispersion interactions was accounted for empirical correction D2 (denoted as PBE+D2) [21] as implemented in Vienna *Ab initio*

Simulation Package (VASP) [22,23]. PAW pseudopotentials were employed, [24,25] and the valence wave functions were expanded in a plane-wave basis with a cutoff energy of 415 eV. The Brillouin zone was sampled using the Γ point only. [26]

2.4.1 Structure modelling of pure silica and copper-containing MFI zeolites

The framework structure of the Si-MFI sample was modeled using an orthorhombic unit cell consisting of 96 T-atoms with the following unit cell parameters: a = 20.271 Å, b = 19.925 Å, c = 13.332 Å. All the T-atoms in the model were silicon. In order to create a local imperfection (*i.e.,* a silanol nest composed of four silanols), one silicon center was removed from the structure, and all the adjacent oxygen atoms were saturated by hydrogen atoms. In order to reach the geometry optimization, all atoms were allowed to relax until the forces on each atom were less than 5×10^{-1} eV/nm. The model structure corresponding to the Si-MFI sample was used and the Cu-species were introduced to simulate the formation of Cu-containing MFI zeolites.

2.4.2 Calculations of the vibrational frequencies for nitrogen monoxide (NO) molecules adsorbed on MFI nanosized zeolites

The N-O vibrational frequencies were calculated using a normal mode analysis where the elements of the Hessian were approximated as finite differences of gradients, displacing each atomic center by 1.5×10^{-3} nm either way along each Cartesian direction. The reported binding energies (*BE*) of the NO adsorbates were calculated based on $BE = -E_{ad}-E_{sub}+E_{ad/sub}$, where E_{ad} is the total energy of the adsorbate in the gas phase (ground state), E_{sub} is the total energy of the pristine zeolite system, and $E_{ad/sub}$ is

the total energy of the zeolite, together with the adsorbate in the optimized geometry. With the above definition, negative values of *BE* imply favorable interactions.

3. Results and Discussion

In this work, EDTA and NH_3 were used as ligands for the synthesis of nanosized copper-containing MFI nanosized zeolites and the samples are denoted as Cu-MFI-EDTA and Cu-MFI-NH_3, respectively. By finely tuning the synthesis conditions, the copper-containing samples were synthesized with almost the same amount of copper, *i.e.* 0.58 wt% and 0.57 wt% for samples Cu-MFI-EDTA and Cu-MFI-NH_3, respectively (see Experimental Section). For comparison, pure siliceous reference sample denoted as Si-MFI was also synthesized. All samples were calcinated at 550 ^{o}C before being characterized (**Table 1**).

3.1 Reduced water affinity and decrease of silanols due to the Cu species insertion into MFI framework

Reduced water affinity of Cu-MFI-EDTA over Si-MFI sample was demonstrated by thermogravimetry **(Fig. 1(A))**. In order to guarantee the identical conditions for the water vapor adsorption measurements, the two samples were pre-dehydrated and then stored at 25 ^{o}C for 72 hours in a desiccator with 58 % relative humidity. The two copper-containing zeolites show decreased water amount compared with the reference sample Si-MFI (4 %), while both Cu-MFI-EDTA and Cu-MFI-NH_3 samples contain similar amount of Cu as determined by ICP-AES (**Table S1 in Supporting Information**). The variation of water content in samples Cu-MFI-EDTA and

Cu-MFI-NH_3 indicates the reduction of silanol groups resulted from the use of copper ligands as confirmed by *in situ* FTIR spectroscopy **(Fig. 1(B))**. The IR spectrum of the reference Si-MFI zeolite contains two absorption bands at 3740 cm^{-1} (terminal silanol groups) and 3520 cm^{-1} (silanol nests),[27] indicating the presence of silanols though it is highly crystalline (*vide infra*) and pure siliceous sample. While in the spectrum of sample Cu-MFI-NH_3, the peak corresponding to silanol nests appears with very low intensity and the peak corresponding to the terminal silanol groups shows diminished intensity too. Whereas for sample Cu-MFI-EDTA, the band at 3520 cm^{-1} is not present and the band at 3740 cm^{-1} with very low intensity corresponding to the terminal silanol is observed. The results above suggest that the water adsorption capacity of the Cu-MFI-EDTA and Cu-MFI-NH_3 samples is decreased by introducing copper with the help of the two ligands in the silanol sites. For sample Cu-MFI-EDTA, a considerable decrease of the silanol nests and complete elimination of the terminal silanol groups indicates less amount of defect sites within the crystals.

[INSERT FIG.1 HERE]

The reduced amount of silanol groups suggests that copper species can be introduced into the framework of the MFI zeolite with the help of EDTA as a ligand, which can be verified by ^{29}Si MAS NMR and related $\{^{1}H\}$-^{29}Si CP MAS NMR spectra (**Fig. 2**). For both samples Si-MFI and Cu-MFI-NH_3, two peaks at -113 ppm and -115 ppm with a shoulder at -111 ppm, all related to the presence of Q^4 species ($(SiO)_4Si$), are measured by ^{29}Si MAS NMR. An additional Q^3 signal ($(SiO)_3SiOH$) at -103 ppm is also detected

for both samples Si-MFI and Cu-MFI-NH_3 (**Fig. 2(A)**). Even an extremely weak Q^2 signal ($(SiO)_2Si(OH)_2$) at -93 ppm appears in the spectrum of the reference sample Si-MFI. The Q^2 and Q^3 species reveal the presence of silanols with unsaturated coordination in both samples, more pronounced for the reference pure silica sample Si-MFI. In contrast, the Q^4 signals in the ^{29}Si MAS NMR spectrum of sample Cu-MFI-EDTA are well resolved, and at least eight peaks ranging from -110 ppm to -120 ppm clearly appeared, which can be explained by a structure with very few silanols.[10] In addition to the well-resolved Q^4 signals, another weak signal at -102 ppm appears in the spectrum of Cu-MFI-EDTA. However, no apparent signals in the $\{^1H\}$-^{29}Si CP MAS NMR spectrum of sample Cu-MFI-EDTA are observed (**Fig. 2(B)**). The appearance of this peak indicates that some of the silicon atoms in this sample are bonded to another three silicon atoms plus one non-silicon atom via oxygen bridge bonds (denoted as $(SiO)_3$-Si-O-X hereafter, where X refers to the non-silicon atom). According to the Cu-MFI-EDTA synthesis recipe, the potential candidate for X atom can be either hydrogen and/or copper. Nevertheless, if X atom were hydrogen atom, a Q^3 peak should appear in the $\{^1H\}$-^{29}Si CP MAS NMR spectrum of Cu-MFI-EDTA, just like the corresponding peak shown in the spectrum of Si-MFI. However, such a peak is not observed in the $\{^1H\}$-^{29}Si CP MAS NMR spectrum of sample Cu-MFI-EDTA (**Fig. 2(B)**), indicating that the X atom could be Cu. The Si MAS NMR and related $\{^1H\}$-^{29}Si CP MAS NMR spectra indicate that the copper species in this case are highly probable to be connected to the silicon via oxygen bridge (Si-O-Cu).

Such results are consistent with the previous reports on tungsten containing (W-MFI)[14] and molybdenum containing (Mo-MFI)[15] zeolites. Besides, the absence of peaks in $\{^{1}H\}$-^{29}Si CP MAS NMR spectrum of sample Cu-MFI-EDTA also indicates the low affinity to proton-containing species like water.

[INSERT FIG.2 HERE]

The insertion of copper atoms in the MFI framework with the help of the EDTA ligand is further evidenced by the crystal symmetry change from orthorhombic to monoclinic for the MFI framework as shown in powder X-ray diffraction patterns (**Fig. 3**). The peak at 24.5^{o} 2 theta in the XRD pattern of sample Cu-MFI-EDTA splits, whereas only one single peak appears in both samples Cu-MFI-NH_3 and Si-MFI. This indicates the space group transformation from orthorhombic *Pnma* (Si-MFI and Cu-MFI-NH_3) to monoclinic $P2_1/c$ (Cu-MFI-EDTA), inferring the symmetry downgrading originated from the introduction of copper into the MFI framework. Compared with the reference sample Si-MFI, the Bragg peaks in the XRD pattern of sample Cu-MFI-EDTA (22-23^{o} 2 Theta) are shifted. The unit cell parameters derived from Le Bail refinement of the three patterns corresponding to samples Si-MFI, Cu-MFI-EDTA, and Cu-MFI-NH_3 are summarized **Table 1**. The unit cell volume increases from 5337.1 $Å^3$ for Si-MFI to 5340.5 $Å^3$ for Cu-MFI-NH_3 and to 5352.0 $Å^3$ for Cu-MFI-EDTA.

[INSERT FIG. 3 HERE]

[INSERT TABLE 1 HERE]

The addition of Cu into the zeolite crystal framework of Cu-MFI-EDTA sample is also confirmed by Raman (**Fig. 4**) and FTIR (**Fig. 5**). Two weak bands symmetrically located on both sides of the peak centered at 380 cm^{-1} (*c.a.* 330 and 420 cm^{-1}, **Fig. 4(B)**) and a new band at 1038 cm^{-1} (**Fig. 4(C)**) for sample Cu-MFI-EDTA are clearly observed. These peaks correspond to the M-O-Si vibration as reported previously for Ti-, Fe-, W-, Mo-containing silicalite-1.[14,15,29] On the contrary, a band at 980 cm^{-1} present in both the Raman (**Fig. 4(C)**) and FTIR (**Fig. 5**) spectra of Cu-MFI-NH_3 and Si-MFI, which is assigned to the O_3Si-OH stretching mode of silanol groups, does not present in the spectra of sample Cu-MFI-EDTA. Such results further confirm silanols removal from sample Cu-MFI-EDTA and is consistent with the results drawn from ^{29}Si MAS NMR and {^{1}H}-^{29}Si CP-MAS NMR study for both Si-MFI and Cu-MFI-EDTA samples.

[INSERT FIG. 4 HERE]

[INSERT FIG. 5 HERE]

3.2 Role of EDTA ligand on healing silanols and promoting Cu species insertion in MFI framework

The distinctive differences between samples Cu-MFI-EDTA and Cu-MFI-NH_3 clearly demonstrate the exceptional functions of the EDTA as a ligand for reinforcing the copper atoms insertion into the MFI framework and simultaneously curing the silanols. In order to unravel the role of the EDTA in the insertion of copper species in the zeolite framework, scanning transmission electron microscopy (STEM) images acquired in

high angular annular dark field (HAADF) and energy dispersion spectroscopy (EDS) show topographical features and Cu dispersion information for sample Cu-MFI-EDTA (**Fig. 6**). Zeolite nanoparticles in sample Cu-MFI-EDTA are round-shaped with rather smooth surface (**Fig. 6(A)-6(E)**). The HAADF-STEM pictures showed the presence of white spots in the zeolite crystals marked by the yellow arrows and circles in **Fig. 6(B)-6(D)**. The corresponding magnified images are supplied in **Fig. S3(A)-S3(C), Supporting Information**, respectively) and the high contrast in the STEM-EDS mapping (green area) is seen in **Fig. 6(H)**. Most of the bright spots associated with the presence of high *Z*-contrast atoms are sited in the lattice fringes of the zeolite crystals (**Fig. 6(D)**. The corresponding magnified images are supplied in **Fig. S3(C), Supporting Information**), indicating that the Cu species are incorporated in the MFI framework, which is in a good correspondence with the NMR (**Fig. 3**), XRD (**Fig. 4**), and theoretical results (*vide infra*). In order to confirm the abovementioned description, the UV-vis spectroscopic study of the Cu-MFI-EDTA was conducted (**Fig. 7**). The UV-vis spectrum of sample Cu-MFI-EDTA contains a peak centered at *c.a.* 260 nm (**Fig. 7(A)**). This peak is assigned as the charge transfer transitions between oxygen in the zeolite crystal lattice to isolated copper species. ($O^{2-} \rightarrow Cu^{2+}$ ligand to metal charge transfer, LMCT). [30,31] No other bands assigned to the d-d transition of $[Cu^{\delta+} \cdots O^{\delta-} \cdots Cu^{\delta+}]_n$ species appear in the region 350 nm - 800 nm. [30,31] Considering that crystallization time of the sample determines the amount of Cu species incorporated in the zeolite framework (**Table S3**, **Supplementary**

Information), further investigation of the changes of the abovementioned absorption peaks vs the amount of the incorporated Cu species in Cu-MFI-EDTA sample was performed **(Fig. 7(B) and 7(C))**. With increasing the copper content in sample Cu-MFI-EDTA, the intensity of the "$O^{2-}\rightarrow Cu^{2+}$ LMCT" absorption peak gradually increases and undergoes a blue shift in the corresponding UV-vis spectra. Based on these results, it can be inferred that the copper species of sample Cu-MFI-EDTA should be in the form of Si-O-Cu, rather than extra framework $[Cu^{\delta+}\cdots O^{\delta-}\cdots Cu^{\delta+}]_n$ clusters.

In contrast with sample Cu-MFI-EDTA, the high-resolution STEM-HAADF study reveals that the Cu-MFI-NH_3 zeolite is highly coarse (**Fig. 6(I)-6(L)**). High-resolution STEM-HAADF and the STEM-EDS analyses indicate that the folded outer surface are prone of being decorated by the copper species (yellow circles shown in **Fig. 6(K) and 6(L),** and the corresponding magnified images are supplied in **Fig. S3(D)-S3(E), Supporting Information**). Although the UV-vis spectrum of sample Cu-MFI-NH_3 does not contain the peak centered at *c.a.* 260 nm, there is an apparent band at wavenumber larger than 550 nm showing the existence of extra framework $[Cu^{\delta+}\cdots O^{\delta-}\cdots Cu^{\delta+}]_n$ cluster species.(**Fig.7(A)**). Considering the *Pmna* space group (a single peak at 24.5^o 2 theta in the XRD pattern shown in **Fig. 3(C)**) and Si-O-H interactions (the Q^3 signal in the $\{^1H\}$-^{29}Si CP-MAS NMR spectrum shown in **Fig. 2(A)**) of sample Cu-MFI-NH_3, one can conclude that the Cu species are solely located at the outer surface of the sample as extra framework $[Cu^{\delta+}\cdots O^{\delta-}\cdots Cu^{\delta+}]_n$ cluster species.

[INSERT FIG. 6 HERE]

[INSERT FIG. 7 HERE]

The unique role of EDTA in implanting the copper species into zeolite framework is also analyzed via *in situ* FTIR study using nitrogen monoxide (NO) as a probe molecule to differentiate the copper species on both Cu-MFI-EDTA (**Fig. 8(A)**) and Cu-MFI-NH_3 (**Fig. 8(B)**) samples. The theoretical calculations for NO adsorbed on both Cu-MFI-EDTA and Cu-MFI-NH_3 samples were performed for better interpretation of the interactions among the copper species, silanol groups and NO probe molecules. Detailed results are summarized in **Table S2 in Supporting Information**. Solely a wide band in the region 1940-1850 cm^{-1} in the IR spectrum of Cu-MFI-EDTA is present (**Fig. 8(A)**). This band corresponds to the N-O stretching vibration and infers the presence of physically adsorbed NO [32,33]. Such assignment is also confirmed by theoretical calculation and shown as inset of **Fig. 8(A)**. The binding energy of physically adsorbed NO is -114 kJ/mol, which is much lower than the nitrosyl complexes, in particular 90 kJ/mol lower than the complex of NO with extra-framework Cu^{2+} cation. Therefore, the absence of the peaks for nitrosyl species in sample Cu-MFI-EDTA suggests that there are no cationic extra-framework copper species in this sample.

On the contrary, in the *in situ* IR spectrum of sample Cu-MFI-NH_3, four apparent peaks from 1950 cm^{-1} to 1840 cm^{-1} appeared (**Fig. 8(B)**). The corresponding theoretical calculation confirms that such four peaks are assigned to the NO adsorption on the

following four copper species in Cu-MFI-NH_3 sample, with binding energy ranging from -123 to -205 kJ/mol: (1) Structure where Cu^{2+} cation compensates two deprotonated silanol groups (denoted as SN-Cu1): the cation interacts not only with them, but also with one of the two intact silanols; (2) Structure where initially two extra-framework Cu^{2+} cations compensate two deprotonated silanol groups in the silanol nest (denoted as SN-Cu2): in the optimized geometry, the silanol nest is healed by one of the copper cations, which is incorporated in the zeolite framework, while the other one remains as a charge compensating Cu^{2+} cation; (3) Structure with neutral extra-framework copper-containing species $Cu^{2+}O^{2-}$, located inside the zeolite channel close to a silanol nest (denoted as SN-CuO): interestingly, during the optimized geometry, such $Cu^{2+}O^{2-}$ species interact with one of the H^+ cations originated from a silanol group, thus $Cu^{2+}OH^-$ species and deprotonated SiO^- group are formed; (4) Structure with neutral extra-framework copper-containing species $Cu^{2+}(OH^-)_2$, also located inside the zeolite channel close to a silanol nest (denoted as SN-$Cu(OH)_2$). Obviously, none of the above four modes point to the existence of copper species inserted in the framework of Cu-MFI-NH_3 sample.

[INSERT FIG. 8 HERE]

3.3 Effect of calcination and presence of sodium cations on the copper species in the zeolite framework

All above results indicate that the less water adsorption capacity of sample Cu-MFI-EDTA is attributed to the introduction of atomically dispersed copper species

into the silanol sites of the MFI zeolite. All samples presented up to now are characterized after the calcination. Considering the pivotal roles during zeolite synthesis, it is necessary to understand the relationship between the calcination and the silanols healing effect. Therefore, the XRD patterns of as-synthesized and calcined Cu-MFI-EDTA samples are compared (**Fig. 9**). After the calcination, the position of the Bragg peaks shifts downwards. Besides, in the calcined Cu-MFI-EDTA sample the peaks at 23.3^{o} and 24.5^{o} 2 theta split (**Fig. 9(A)**). Correspondingly, the FTIR spectra also show that the band at 980 cm^{-1} (silanol sites in zeolite framework, **Fig. 9(B)**) disappeared during the calcination process. This indicates that the silanol sites are healed during the calcination of the Cu-MFI-EDTA sample.

[INSERT FIG. 9 HERE]

Due to the low solubility of H_2EDTA, the disodium salt form, Na_2EDTA, is instead chosen for introducing the EDTA ligand into the synthesis. Therefore, it is of interest to investigate the effect of sodium cations on the formation of the Cu-MFI-EDTA and the location of the Cu-EDTA chelate. The possibility for confining the Na_2[Cu-EDTA] coordination compound in the channel intersections of MFI framework in vicinity of the silanol nests was modeled; this corresponds to the as-synthesized Cu-MFI-EDTA sample. The structure was optimized, which suggests that the bulky coordination compound can be well accommodated in the zeolite channels (**Fig. 10(A)**). Interestingly, the incorporation of the bulky compound does not affect the zeolite framework, which remains essentially unchanged, except the hydroxyl groups in the

silanol nests. The Si-Si distance of the structure with and without Na_2[Cu-EDTA] is shown in **Fig. S4**. The coordination compound itself is sufficiently flexible, as shown earlier,[34] and this allows to fit in the available channel intersection. The calculated binding energy with respect to isolated Na_2[Cu-EDTA] coordination compound and empty zeolite model is large (-317 kJ/mol). In order to understand the effect of additional sodium cations, an MFI zeolite consisting of 96 Si atoms was constructed as a basic model structure for accommodating the guest Cu-containing species. The results show that the Cu^{2+} cation can be incorporated into the zeolite framework at the position of the silanol nest. Two charge-compensating Na^{+} cations from the Na_2[Cu-EDTA] are located in the vicinity, which is consistent with the Cu/Na molar ratio close to 0.5 shown in **Table S1**, i.e. 0.58 wt % and 0.43 wt % for Cu and Na in sample Cu-MFI-EDTA respectively. Thus, all four protons from the silanol nest hydroxyls are replaced by copper or sodium ions. Among them, three of the oxygen centers from the silanol groups are coordinated to the copper ion while the sodium cations are coordinated to the fourth oxygen center and surrounding oxygen atoms (**Fig. 10(B)**).

[INSERT FIG. 10 HERE]

Based on the abovementioned results, a possible explanation on the unique function of the Cu-EDTA complex (sample Cu-MFI-EDTA) on healing the silanols is presented (**Scheme 1**). Silanols are unavoidably created during the crystallization of nanosized zeolites. For the synthesis of nanosized Cu-MFI-EDTA zeolite, the used aqueous

precursor suspension is highly alkaline: the pH value of the precursor suspension after adding the EDTA is 13.75 (**Table S1**). Under such condition, the EDTA mainly exists in the form of $EDTA^{4-}$ ion, with a distribution coefficient in aqueous solution not less than 0.998.[35,36] Due to the chelate effect of $EDTA^{4-}$ ion and the help of Na^{+} as counter cation, Cu^{2+} exclusively forms Na_2[Cu-EDTA] complex stoichiometrically with a ratio of 1:1, regardless of the initial molar ratio between Cu^{2+} and $EDTA^{4-}$. Based on the theoretical result, the Na_2[Cu-EDTA] coordination compound is prone of being confined in the channel intersections of MFI frameworks. When the confined Na_2[Cu-EDTA] is in vicinity of the silanol nests, Cu species becomes part of the MFI framework by forming flexible Cu-O-Si bonds. In contrast, the [Cu-NH_3] cannot be finely fixed and confined within the channel intersections of the MFI framework. In this case, the copper species in Cu-MFI-NH_3 sample only exist in the form of various extra-framework clusters $[Cu^{\delta+}\cdots O^{\delta-}\cdots Cu^{\delta+}]_n$ and do not have the ability to repair the silanol-based defects of the Cu-MFI-NH_3 sample. From this point of view, Na_2EDTA can achieve the purpose of healing silanols of nanosized MFI zeolites, while introduction of ammonia as ligand cannot play such a role even though it also does promote the solubility of copper species in the synthesis mixture (see **Fig. S1(B)and S1(C)**)

[INSERT SCHEME 1 HERE]

4. Conclusions

Copper containing nanosized MFI zeolite crystals with reduced water affinity were synthesized via one-pot synthesis method. The addition of Na_2EDTA ligand into the synthesis suspension guarantees the formation of octahedral Na_2[Cu-EDTA] coordination compound that is likely to be confined in the channel intersection of MFI framework or deposited on the outer surface. During the calcination, the confined Na_2[Cu-EDTA] in vicinity of the silanol nests become part of the MFI framework via flexible Cu-O-Si interactions and heal the silanols with the help of sodium cations. On the contrary, the [Cu-NH_3] compounds cannot be confined within zeolite channel intersections, leading to various extra-framework $[Cu^{\delta+}\cdots O^{\delta-}\cdots Cu^{\delta+}]_n$ clusters that cannot cure the silanols of the Cu-MFI-NH_3 sample.

References

[1] J. Čejka, H. Van Bekkum, A. Corma, F. Schüth, Introduction to zeolite molecular sieves, Elsevier, 2007.

[2] Y. Li, L. Li, J. Yu, Applications of Zeolites in Sustainable Chemistry, Chem. 3 (2017) 928–949.

[3] S. Mintova, J. Grand, V. Valtchev, Nanosized zeolites: Quo Vadis?, Comptes Rendus Chim. 19 (2016) 183–191.

[4] L.-H. Chen, M.-H. Sun, Z. Wang, W. Yang, Z. Xie, B.-L. Su, Hierarchically Structured Zeolites: From Design to Application, Chem. Rev. 120 (2020) 11194–11294.

[5] P. Peng, X.-H. Gao, Z.-F. Yan, S. Mintova, Diffusion and catalyst efficiency in hierarchical zeolite catalysts, Natl. Sci. Rev. 7 (2020) 1726–1742.

[6] E. Dib, J. Grand, S. Mintova, C. Fernandez, Structure-Directing Agent Governs the Location of Silanol Defects in Zeolites, Chem. Mater. 27 (2015) 7577–7579.

[7] C.E. Ramachandran, S. Chempath, L.J. Broadbelt, R.Q. Snurr, Water adsorption in hydrophobic nanopores: Monte Carlo simulations of water in silicalite, Microporous Mesoporous Mater. 90 (2006) 293–298.

[8] A. Özgür Yazaydın, R.W. Thompson, Molecular simulation of water adsorption in silicalite: Effect of silanol groups and different cations, Microporous Mesoporous Mater. 123 (2009) 169–176.

[9] S. Dzwigaj, M.J. Peltre, P. Massiani, A. Davidson, M. Che, S. Dzwigaj, P. Massiani, T. Sen, S. Sivasanker, Incorporation of vanadium species in a dealuminated β zeolite, Chem. Commun. (1998) 87–88.

[10] M. Trzpit, M. Soulard, J. Patarin, N. Desbiens, F. Cailliez, A. Boutin, I. Demachy, A.H. Fuchs, The Effect of Local Defects on Water Adsorption in Silicalite-1 Zeolite: A Joint Experimental and Molecular Simulation Study, Langmuir. 23 (2007) 10131–10139.

[11] E.B. Clatworthy, S. V. Konnov, F. Dubray, N. Nesterenko, J. Gilson, S. Mintova, Emphasis on the Properties of Metal-Containing Zeolites Operating Outside the Comfort Zone of Current Heterogeneous Catalytic Reactions, Angew. Chemie Int. Ed. 59 (2020) 19414–19432.

[12] I.C. Medeiros-Costa, E. Dib, N. Nesterenko, J.P. Dath, J.P. Gilson, S. Mintova, Silanol defect engineering and healing in zeolites: opportunities to fine-tune their properties and performances, Chem. Soc. Rev. 50 (2021) 11156–11179.

[13] J. Grand, S.N. Talapaneni, A. Vicente, C. Fernandez, E. Dib, H.A. Aleksandrov, G.N. Vayssilov, R. Retoux, P. Boullay, J. Gilson, V. Valtchev, S. Mintova, One-pot synthesis of silanol-free nanosized MFI zeolite, Nat. Mater. 16 (2017) 1010–1015.

[14] F. Dubray, S. Moldovan, C. Kouvatas, J. Grand, C. Aquino, N. Barrier, J.-P. Gilson, N. Nesterenko, D. Minoux, S. Mintova, Direct Evidence for Single Molybdenum Atoms Incorporated in the Framework of MFI Zeolite Nanocrystals, J. Am. Chem. Soc. 141 (2019) 8689–8693.

[15] S. V Konnov, F. Dubray, E.B. Clatworthy, C. Kouvatas, J.-P. Gilson, J.-P. Dath, D. Minoux, C. Aquino, V. Valtchev, S. Moldovan, S. Koneti, N. Nesterenko, S. Mintova, Novel Strategy for the Synthesis of Ultra-Stable Single-Site Mo-ZSM-5 Zeolite Nanocrystals, Angew. Chemie Int. Ed. 59 (2020) 19553–19560.

[16] T.W. Hansen, A.T. DeLaRiva, S.R. Challa, A.K. Datye, Sintering of catalytic nanoparticles: particle migration or Ostwald ripening?, Acc. Chem. Res. 46 (2013) 1720–1730.

[17] V.L. Sushkevich, D. Palagin, J.A. van Bokhoven, The Effect of the Active-Site Structure on the Activity of Copper Mordenite in the Aerobic and Anaerobic

Conversion of Methane into Methanol, Angew. Chemie Int. Ed. 57 (2018) 8906–8910.

[18] E. Yuan, K. Zhang, G. Lu, Z. Mo, Z. Tang, Synthesis and application of metal-containing ZSM-5 for the selective catalytic reduction of NO_x with NH_3, J. Ind. Eng. Chem. 42 (2016) 142–148.

[19] L. Ren, L. Zhu, C. Yang, Y. Chen, Q. Sun, H. Zhang, C. Li, F. Nawaz, X. Meng, F.S. Xiao, Designed copper-amine complex as an efficient template for one-pot synthesis of Cu-SSZ-13 zeolite with excellent activity for selective catalytic reduction of NO_x by NH_3, Chem. Commun. 47 (2011) 9789–9791.

[20] J.P. Perdew, K. Burke, M. Ernzerhof, Generalized Gradient Approximation Made Simple, Phys. Rev. Lett. 77 (1996) 3865–3868.

[21] S. Grimme, Semiempirical GGA-type density functional constructed with a long-range dispersion correction, J. Comput. Chem. 27 (2006) 1787–1799.

[22] G. Kresse, J. Hafner, Ab initio molecular-dynamics simulation of the liquid-metal--amorphous-semiconductor transition in germanium, Phys. Rev. B. 49 (1994) 14251–14269.

[23] G. Kresse, J. Furthmüller, Efficiency of ab-initio total energy calculations for metals and semiconductors using a plane-wave basis set, Comput. Mater. Sci. 6 (1996) 15–50.

[24] P.E. Blöchl, Projector augmented-wave method, Phys. Rev. B. 50 (1994) 17953–17979.

[25] G. Kresse, D. Joubert, From ultrasoft pseudopotentials to the projector augmented-wave method, Phys. Rev. B. 59 (1999) 1758–1775.

[26] Y. Jeanvoine, J.G. Ángyán, G. Kresse, J. Hafner, Brønsted Acid Sites in HSAPO-34 and Chabazite: An Ab Initio Structural Study, J. Phys. Chem. B. 102 (1998) 5573–5580.

[27] A. Zecchina, S. Bordiga, G. Spoto, D. Scarano, G. Petrini, G. Leofanti, M. Padovan, C.O. Areàn, Low-temperature Fourier-transform infrared investigation of the interaction of CO with nanosized ZSM5 and silicalite, J. Chem. Soc. Faraday Trans. 88 (1992) 2959–2969.

[28] I.C. Medeiros-Costa, E. Dib, F. Dubray, S. Moldovan, J.P. Gilson, J.P. Dath, N. Nesterenko, H.A. Aleksandrov, G.N. Vayssilov, S. Mintova, Unraveling the Effect of Silanol Defects on the Insertion of Single-Site Mo in the MFI Zeolite Framework, Inorg. Chem. 61 (2022) 1418–1425.

[29] F. Geobaldo, S. Bordiga, G. Spoto, D. Scarano, A. Zecchina, G. Petrini, G. Leofanti, G. Tozzola, M. Padovan, Structure and reactivity of framework and extraframework iron in Fe-silicalite as investigated by optical (IR, RAMAN, DRS UV-Vis) and EPR spectroscopies, in: H.G. Karge, J.B.T.-S. in S.S. and C. Weitkamp (Eds.), Zeolite Sci. 1994 Recent Prog. Discuss., Elsevier, 1995: pp. 112–113.

[30] P. Kaminski, I. Sobczak, P. Decyk, M. Ziolek, W.J. Roth, B. Campo, M. Daturi, Zeolite MCM-22 Modified with Au and Cu for Catalytic Total Oxidation of Methanol and Carbon Monoxide, J. Phys. Chem. C. 117 (2013) 2147–2159.

[31] D. Esquivel, A.J. Cruz-Cabeza, C. Jiménez-Sanchidrián, F.J. Romero-Salguero, Transition metal exchanged β zeolites: Characterization of the metal state and catalytic application in the methanol conversion to hydrocarbons, Microporous Mesoporous Mater. 179 (2013) 30–39.

[32] K. Nakamoto, Infrared spectra of inorganic and coordination compounds, 2nd ed., Wiley, New York, 1970.

[33] K.I. Hadjiivanov, Identification of Neutral and Charged NxOy Surface Species by IR Spectroscopy, Catal. Rev. 42 (2000) 71–144.

[34] M. Ćendić, R.J. Deeth, A. Meetsma, E. Garribba, D. Sanna, Z.D. Matović, Chelating properties of EDTA-type ligands containing six-membered backbone ring toward copper ion: Structure, EPR and TD-DFT evaluation, Polyhedron. 124 (2017) 215–228.

[35] R.M. Smith, A.E. Martell, R.J. Motekaitis, NIST standard reference database 46, 2004.

[36] D.S. Hage, J.D. Carr, Analytical chemistry and quantitative analysis, Prentice Hall Boston, 2011.

Acknowledgement

This work was supported by the IRN "Zeolites", the National Key Technologies R&D Program of China: Key Project of Intergovernmental International Innovation Cooperation (2018YFE0118200), Natural Science Foundation of Shandong Province (ZR2021QB082), Postdoctoral Research Foundation of China (2021M703583), Shandong Provincial Postdoctoral Science Foundation (202102026), Qingdao Postdoctoral Science Foundation (QDYY20200100), Fundamental Research Funds for the Central Universities (21CX06022A), GENESIS (ANR-11-EQPX-0020) and the Label of Excellence "Centre of nanozeolites and related porous materials" supported by Region Normandie. GENESIS is supported by the Région Haute-Normandie, the Métropole Rouen Normandie, the CNRS via LABEX EMC, and the French National Research Agency as a part of the program "Investissements d'avenir". H. A. A. and G. N. V. acknowledge support by the European Regional Development Fund and the Operational Program "Science and Education for Smart Growth" under contract UNITe No. BG05M2OP001-1.001-0004-C01.

Figures and Tables

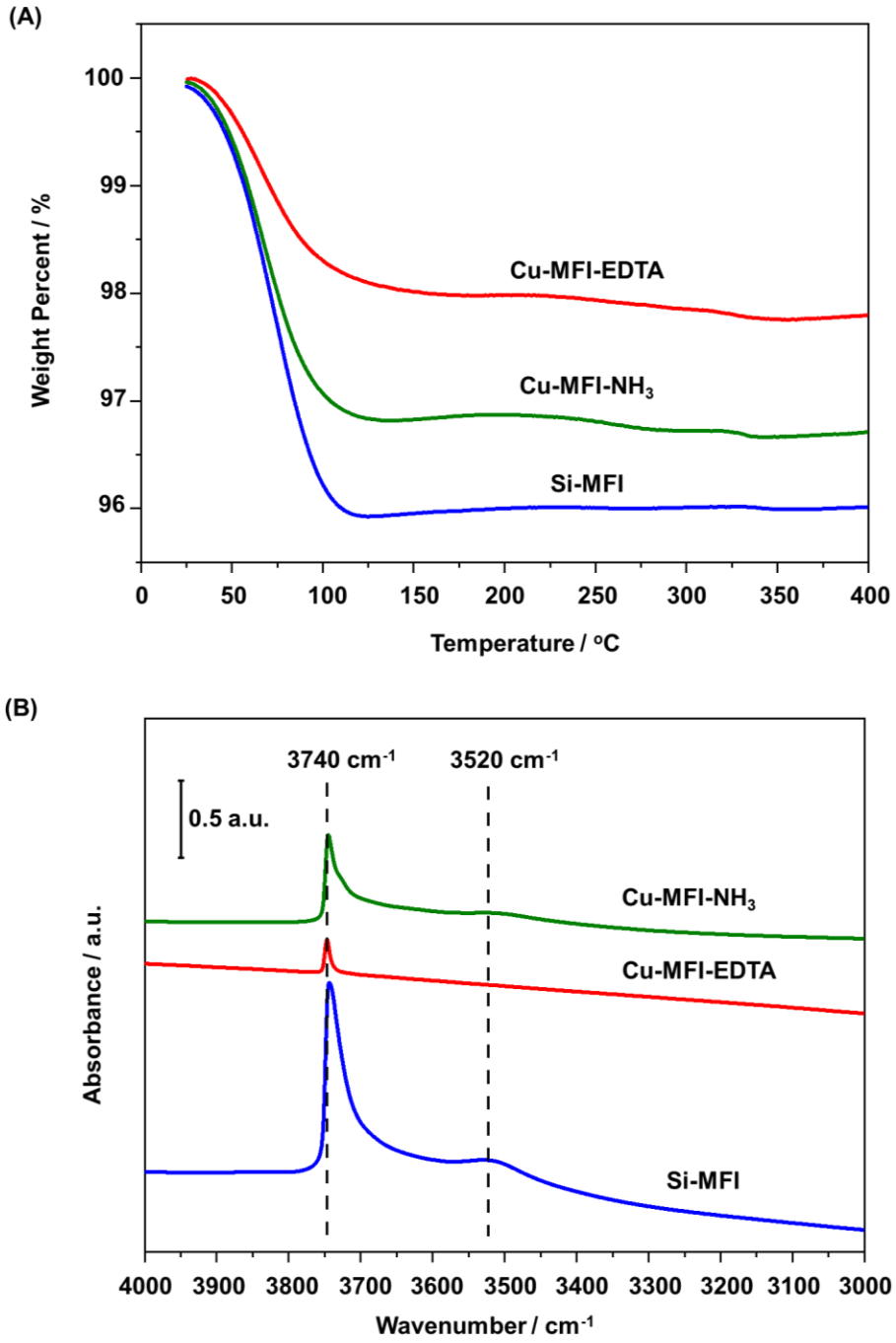

Fig. 1. Water content in calcinated Si-MFI, Cu-MFI-EDTA, and Cu-MFI-NH_3 nanosized zeolites stored at 58 % relative humidity for 3 days measured by

thermogravimetry (A); *In-situ* FTIR spectra of calcined Si-MFI, Cu-MFI-EDTA, and Cu-MFI-NH_3 nanosized zeolites (B) in the region 4000-3000 cm^{-1}.

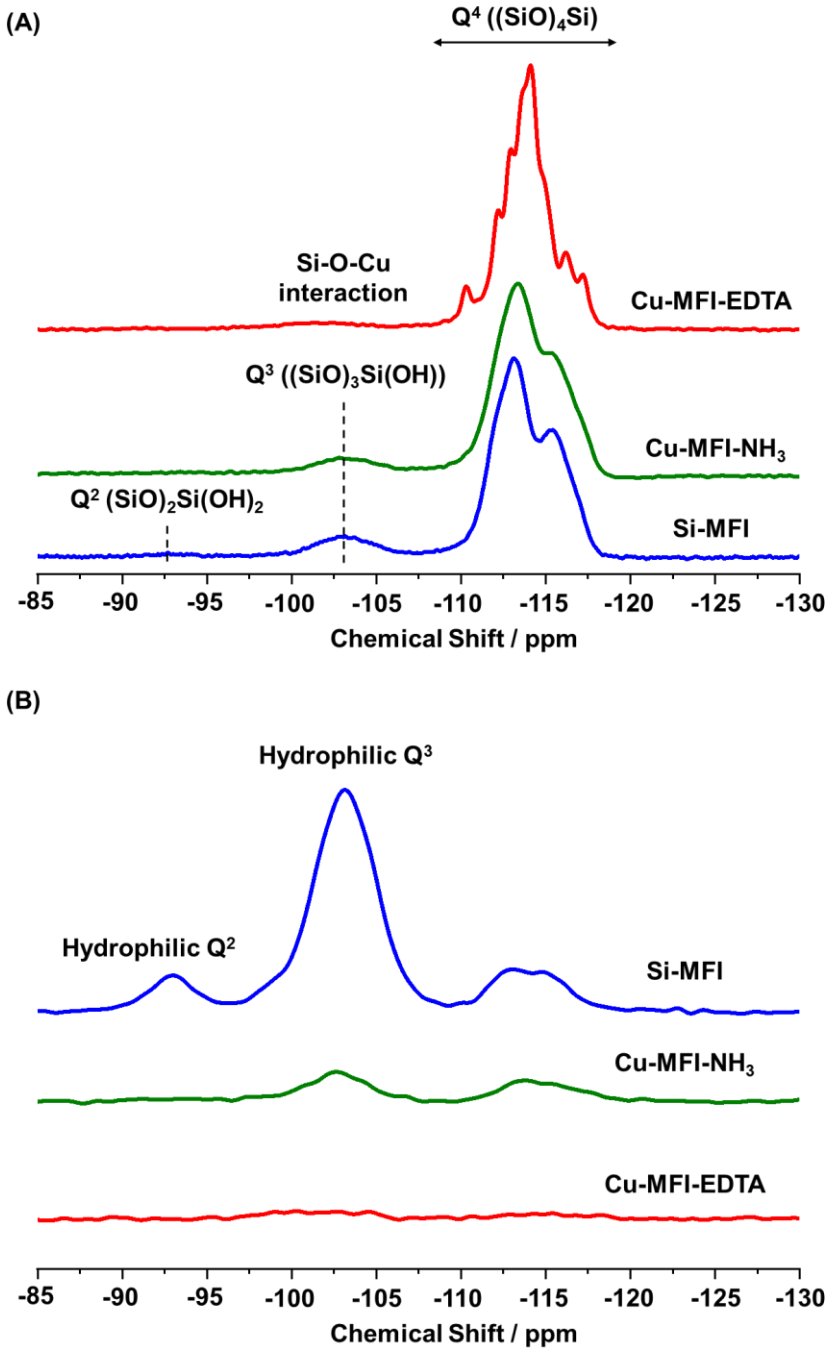

Fig. 2. Solid-state ^{29}Si MAS NMR spectra (A) and the corresponding {^{1}H}-^{29}Si CP-MAS NMR spectra (B) of Si-MFI, Cu-MFI-EDTA, and Cu-MFI-NH_3 nanosized zeolites.

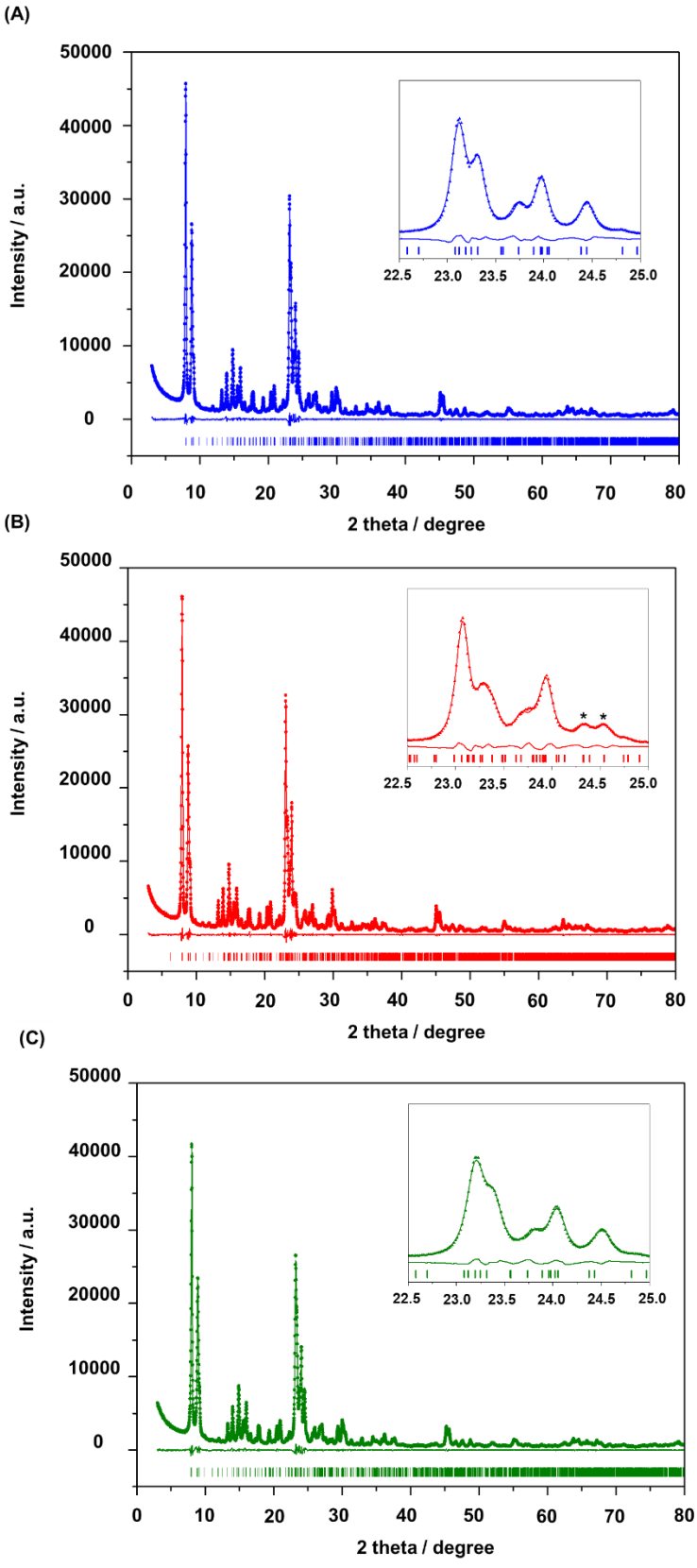
(A)
Intensity / a.u.
2 theta / degree
(B)
Intensity / a.u.
2 theta / degree
(C)
Intensity / a.u.
2 theta / degree

1

Fig. 3. Powder XRD patterns of (A) Si-MFI, (B) Cu-MFI-EDTA, and (C) Cu-MFI-NH_3 calcined nanosized zeolites

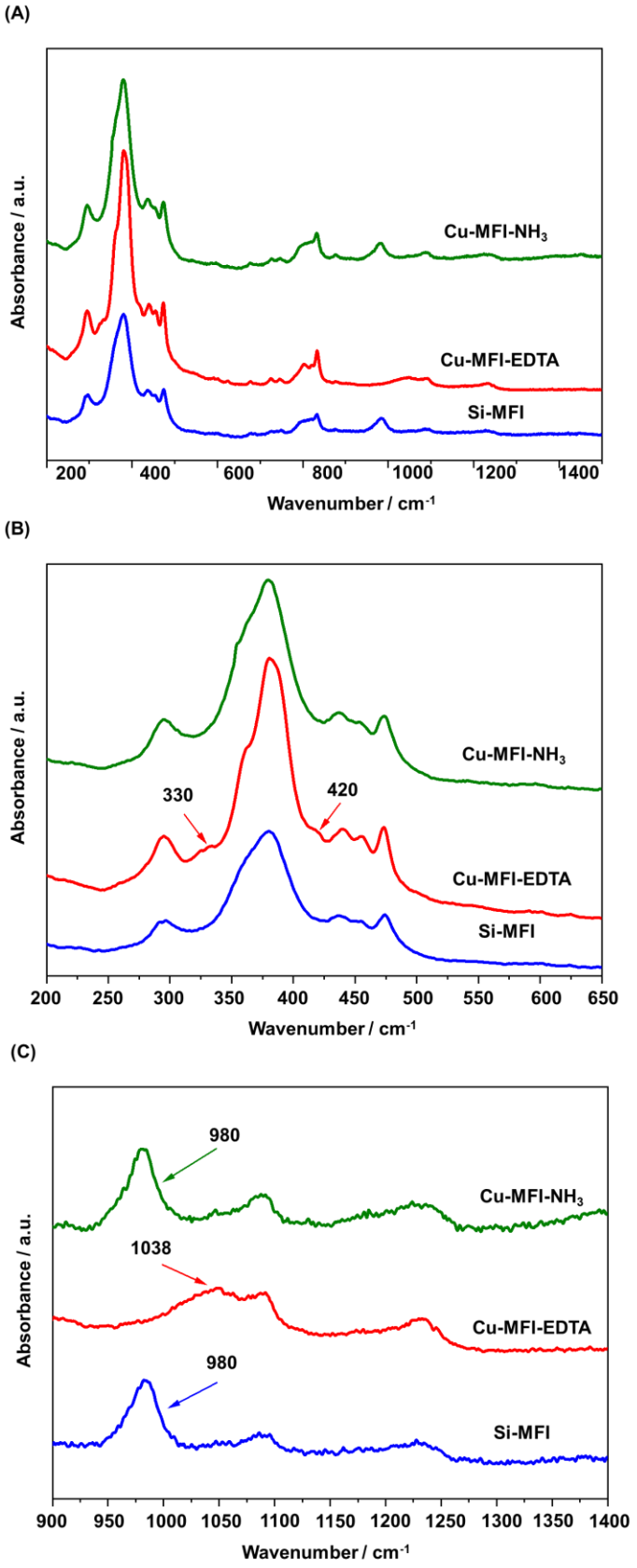
(A)
Absorbance / a.u.
Cu-MFI-NH3
Cu-MFI-EDTA
Si-MFI
200
400
600
800
1000
1200
1400
Wavenumber / cm-1
(B)
Absorbance / a.u.
330
420
Cu-MFI-NH3
Cu-MFI-EDTA
Si-MFI
200
250
300
350
400
450
500
550
600
650
Wavenumber / cm-1
(C)
Absorbance / a.u.
980
1038
980
Cu-MFI-NH3
Cu-MFI-EDTA
Si-MFI
900
950
1000
1050
1100
1150
1200
1250
1300
1350
1400
Wavenumber / cm-1

1

Fig. 4. Raman spectra of Si-MFI, Cu-MFI-EDTA, and Cu-MFI-NH_3 nanosized zeolites in the ranges (A) 200-1500 cm^{-1}(B) 200-650 cm^{-1} (B), and (C) 900-1400 cm^{-1}.

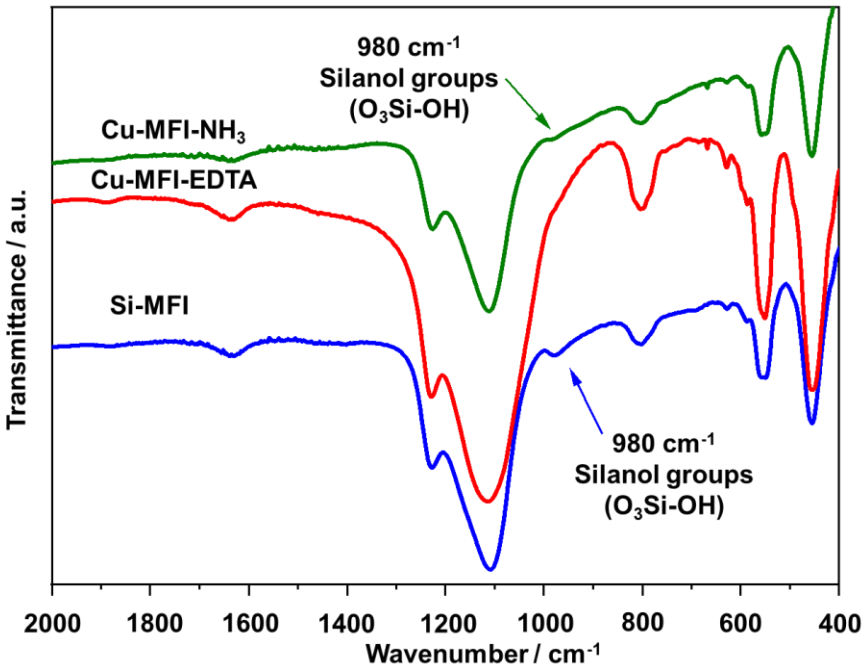

Fig. 5. FTIR spectra of Si-MFI, Cu-MFI-EDTA, and Cu-MFI-NH_3 nanosized zeolites.

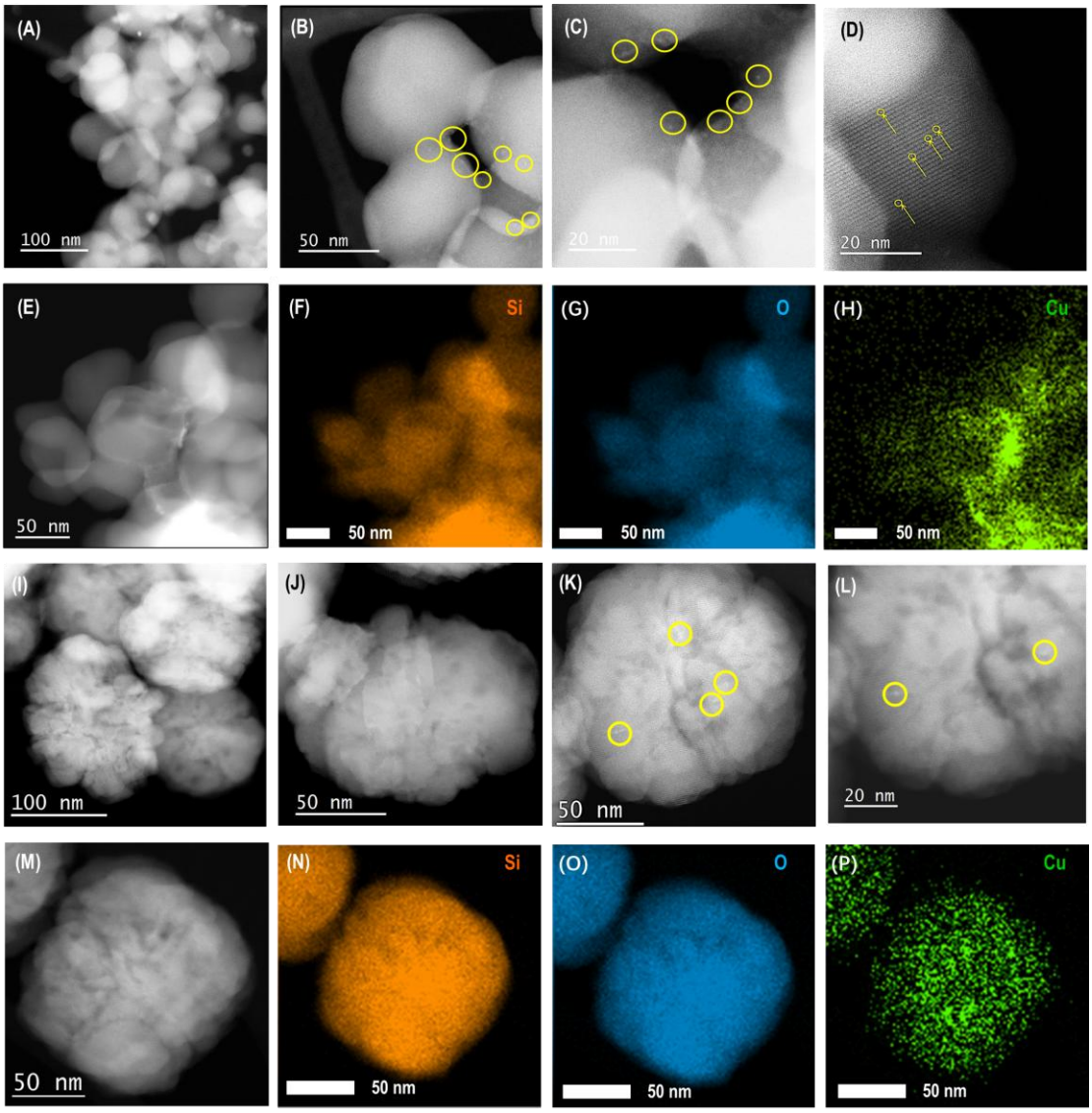

Fig. 6. STEM-HAADF micrographs (A-E, arrows and circles in B-D show the copper species) and STEM-EDS elemental maps (F: Si (orange), G: O (blue), and H: Cu (green)) of Cu-MFI-EDTA nanosized zeolites; STEM-HAADF micrographs (I-M, arrows in J-L show the copper species) and STEM-EDS elemental maps (N-P; N: Si (orange), O: O (blue), and P: Cu (green)) of Cu-MFI-NH_3 nanosized zeolites.

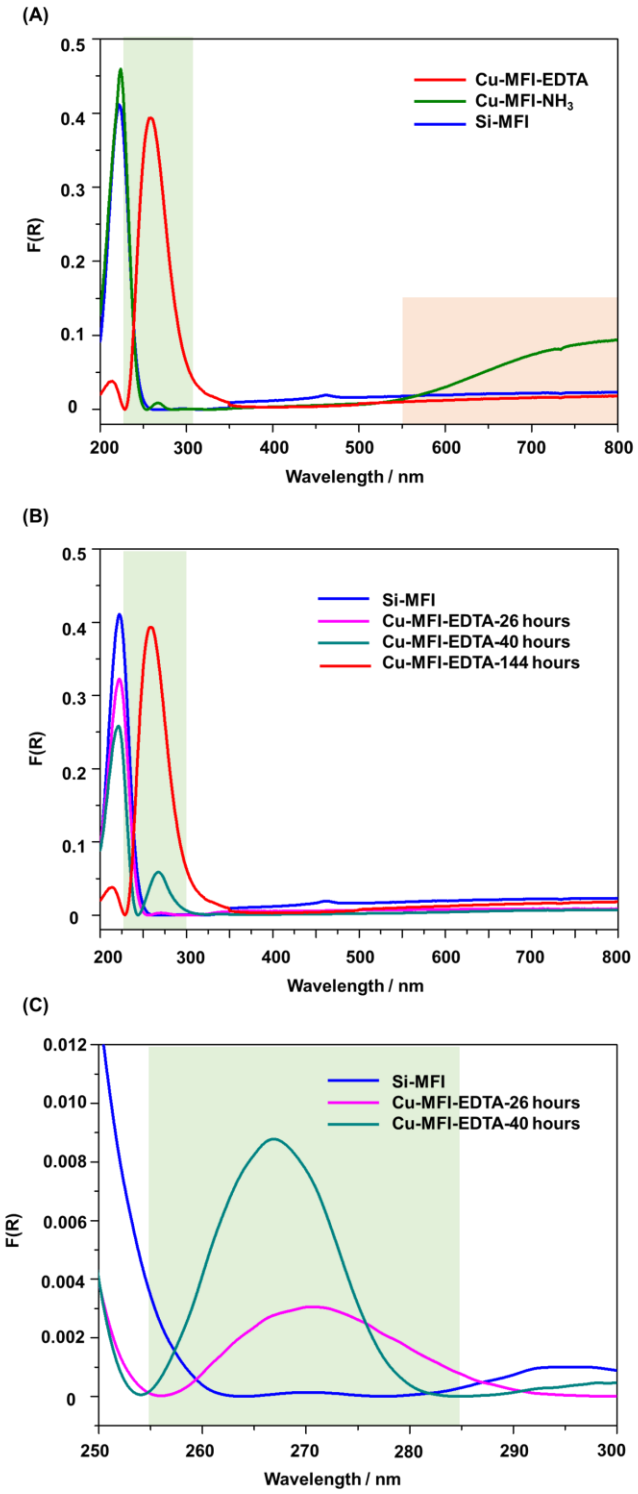

Fig. 7. UV-Vis spectra of Si-MFI, Cu-MFI-EDTA, and Cu-MFI-NH_3 nanosized zeolites in the range of 200-800 nm(A); UV-Vis spectra of Si-MFI, Cu-MFI-EDTA

1 samples after different crystallization time in the ranges (B) 200-800 nm and (C)

2 250-300 nm.

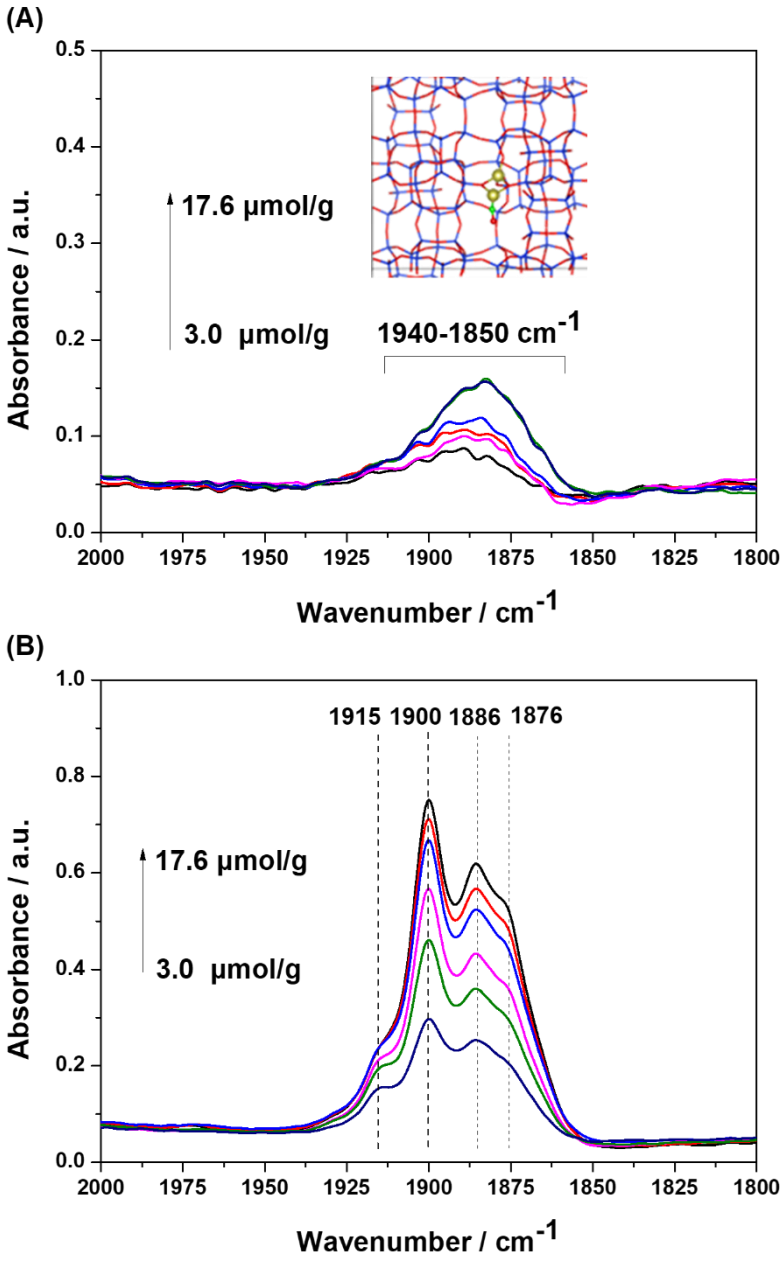

3

4 **Fig. 8.** *In-situ* FTIR spectra of Cu-MFI-EDTA nanosized zeolite recorded at different

5 concentrations of nitrogen monoxide (3.0, 5.9, 8.9, 11.8, 14.7, and 17.6×10^{-3} mmol/g)

6 at room temperature. The inset illustrates the modeled physically adsorbed NO on the

7 Cu-MFI-EDTA nanosized zeolite (A); *In-situ* FTIR spectrum of Cu-MFI-NH_3

nanosized zeolite recorded at different concentrations of nitrogen monoxide (3.0, 5.9, 8.9, 11.8, 14.7, and 17.6×10^{-3} mmol/g) at room temperature. The insets illustrate the modeled adsorbed NO mode on the Cu-MFI-NH_3 nanosized zeolite (B).

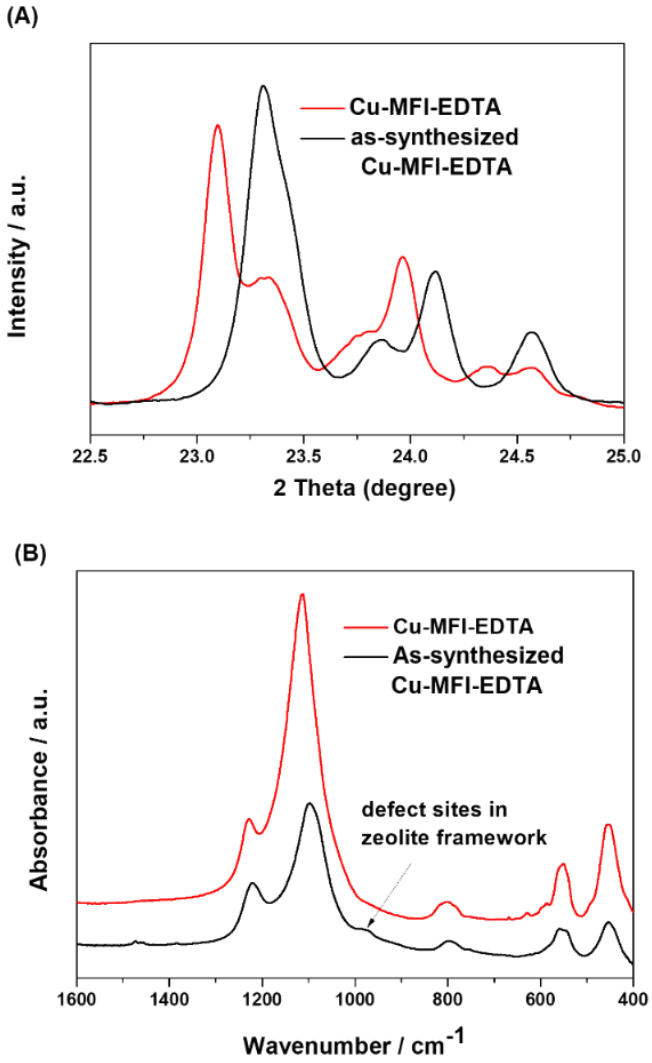

Fig. 9. XRD patterns (A) and FTIR spectra (B) of Cu-MFI-EDTA and Si-MFI nanosized zeolites before and after calcination

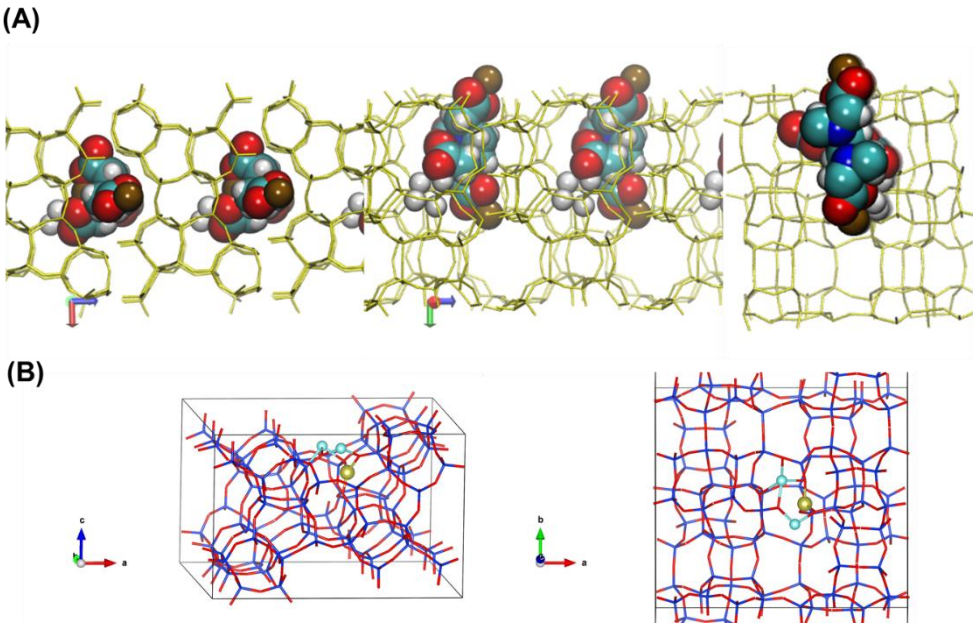

Fig. 10. The Na_2[Cu-EDTA] coordination compound in the channel intersection of MFI zeolite from different points of view (A); location of Cu and Na in the modeled Cu-MFI-EDTA structure from two points of view (B) (Color coding: Si—blue, Cu—yellow, O—red, Na—cyan, N—light yellow, and C—brown).

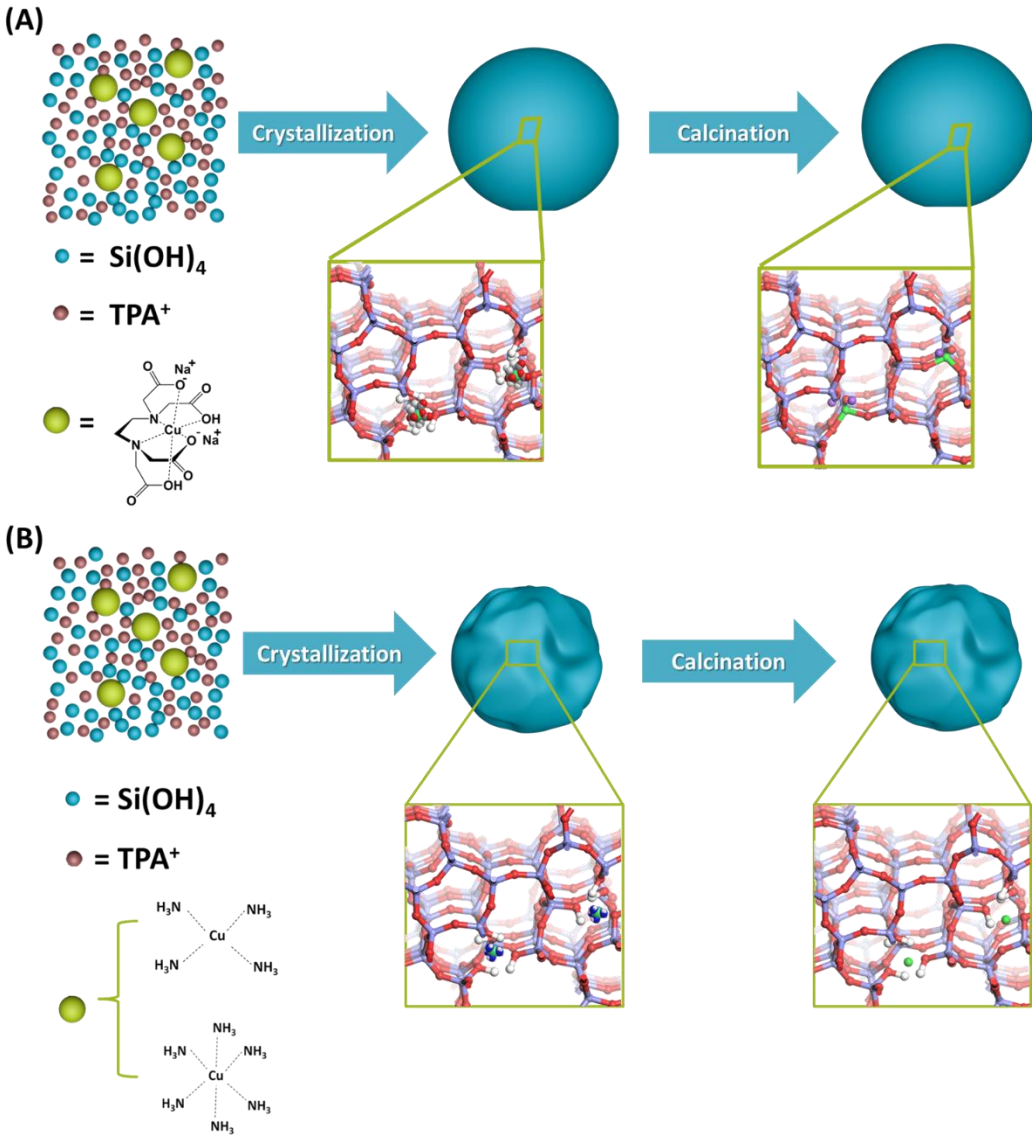

Scheme 1 Graphical illustration of the distinctive effects of the Cu using EDTA (A) or NH_3 (B) as ligands for healing the silanols in nanosized MFI zeolites.

Table 1 Unit cell parameters of nanosized zeolites Si-MFI and Cu-MFI-EDTA. Unit cell parameters were calculated from powder diffraction data based on a Le Bail profile refinement and Pseudo-Voigt profile function using the JANA2006 software.

Sample	Space group	*a* [Å]	*b* [Å]	*c* [Å]	*β* [°]	*V* [Å^3]
Si-MFI	*Pnma*	20.0630	19.8836	13.3788	90.000	5337.1
Cu-MFI-EDTA	$P2_1/n$	20.1129	19.8790	13.3865	90.544	5352.0
Cu-MFI-NH_3	*Pnma*	20.0622	19.8833	13.3876	90.000	5340.5